OPEN ACCESS
Journal of Multidisciplinary Applied Natural Science Vol. xx No. xx (xxxx) https://doi.org/10.47352/jmans.2774-3047.366
Check for updates
Research Article

Subsurface Identification using Horizontal to Vertical Spectral Ratio and Inverse Velocity Modelling in Suoh Pull-apart Basin, Indonesia

Rahmi Mulyasari*, Muh. Sarkowi, Nandi Haerudin, Hari Wiki Utama, Angga Jati Widiatama, I Gede Boy Darmawan, Andri Kurniawan, Yayan Mi'rojul Husni, Hesti Hesti, Nofita Fatmawati, and Serli Marlina

Received : November 26, 2025	Revised : January 16, 2026	Accepted : Februari 6, 2026	Online : March 8, 2026

Abstract
Suoh is a pull-apart basin located along the Semangko segment of the Sumatra Fault Zone and filled by thick fluvio-volcanic and alluvial deposits that strongly amplify seismic waves and increase surface damage during earthquakes. This study aims to perform seismic micro-zonation of Suoh using the horizontal-to-vertical spectral ratio (HVSR) method combined with shallow shear-wave velocity (V_s) inversion to support hazard assessment and land-use planning in the Suoh aspiring geopark. Single station microtremor measurements were acquired at 30 sites and processed with Geopsy to obtain dominant frequency (f_0), amplification factor (A_0), and seismic vulnerability index (K_g). The HVSR curves were further inverted using the Dinver module to retrieve 1D V_s profiles, with initial models constrained by the global CRUST1.0 model and local geology. The results indicate strong lateral variability in site conditions, with low f_0 and high A_0 values concentrated in the central–western basin, producing high K_g and reflecting thick-soft sediments overlying deep engineering bedrock ($V_s \geq 800$ m/s) at depths exceeding 80–100 m. These high-vulnerability zones spatially coincide with shallow seismicity associated with the Semangko Fault. Based on K_g, the study delineates low, moderate, and high seismic vulnerability zones, highlighting areas where seismic amplification and resonance effects are most pronounced. The combination of HVSR parameters with 2D V_s imaging provides a practical framework for identifying high-risk zones and guiding risk-informed land-use planning in tectono-volcanic basins such as Suoh.

Keywords: horizontal-to-vertical spectral ratio, seismic micro-zonation, seismic vulnerability, shear-wave velocity, Sumatra fault zone, Suoh pull-apart basin

1. INTRODUCTION

Indonesia is one of the regions with the most complex seismotectonic setting in the world because it lies at the junction of the Eurasian, Indo-Australian, and Pacific plates [1]. Relative motion between these plates produces extensive subduction zones and active fault systems that can generate large and destructive earthquakes [2]. The impact of an earthquake, however, is not controlled solely by its magnitude or source–to–site distance. Local geological conditions and dynamic soil properties play a crucial role in modifying the amplitude, frequency content, and duration of ground shaking at the surface [3]. Consequently, seismic micro-zonation, which maps spatial variations in local site response, has become an essential component of earthquake risk mitigation and land-use planning [4]-[6].

One of the most important tectonic structures in Indonesia is the Sumatra Fault Zone (SFZ), a ~1,900-km-long right-lateral strike-slip fault system that accommodates a significant portion of the oblique convergence between the Indo-Australian and Eurasian plates [7]. The Semangko segment, located in southern Sumatra, is a key element of this system and is known for its high level of seismic activity [7][8]. Within this segment, the Suoh pull-apart basin is a prominent tectonic feature formed in a step-over zone between overlapping strike-slip faults [7][9]. The basin has a rhomboidal shape and is filled with thick alluvial and fluvio-volcanic deposits derived from the surrounding volcanoes, particularly Mount Sekincau and Mount Seminung, which are expected to strongly influence local seismic site effects [9][10].

Suoh has experienced several damaging earthquakes in the historical record, including the 1933 (Ms 7.5) and 1994 (Mw 7.0) events, which triggered landslides, phreatic eruptions, ground fissures, and liquefaction [11]. These events

Please cite this article as: R. Mulyasari, M. Sarkowi, N. Haerudin, H. W. Utama, A. J. Widiatama, I G. B. Darmawan, A. Kurniawan, Y. M. Husni, H. Hesti, N. Fatmawati, and S. Marlina. (2026). "Subsurface Identification using Horizontal to Vertical Spectral Ratio and Inverse Velocity Modelling in Suoh Pull-apart Basin, Indonesia". *Journal of Multidisciplinary Applied Natural Science*. https://doi.org/10.47352/jmans.2774-3047.366

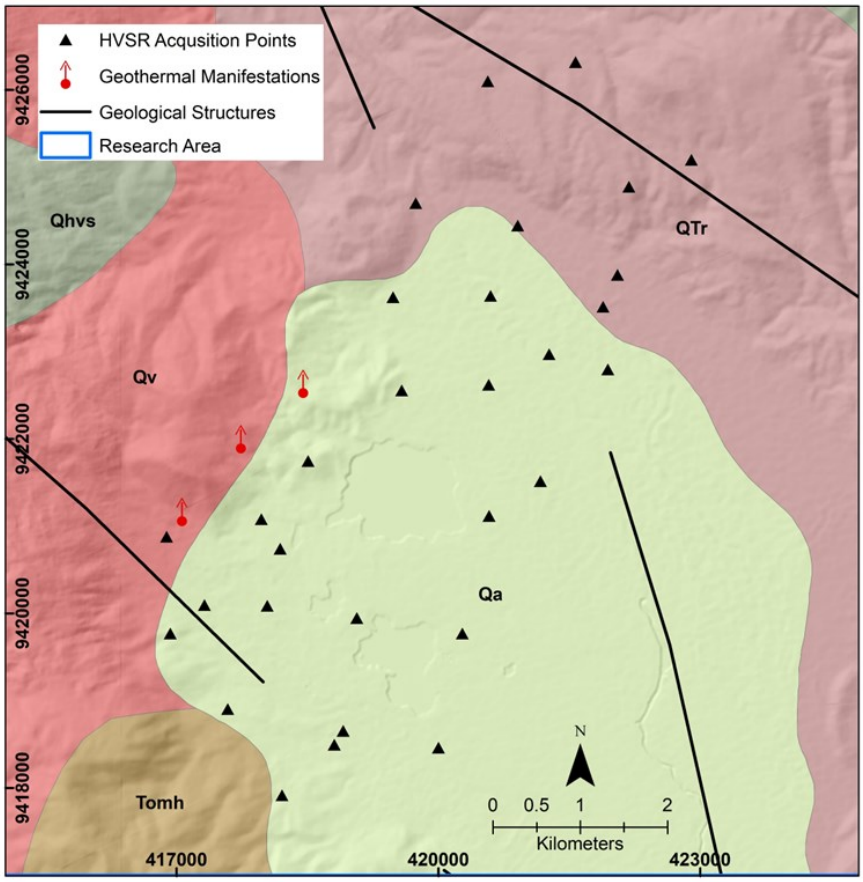

Figure 1. Simplified geological map of the Suoh area showing the main lithological units (Qa, Qv, QTr, Qhvs, Tomh) derived from the regional geological map. Black triangles indicate HVSR acquisition points, red arrows mark geothermal manifestations, and black lines represent mapped geological structures (faults). The blue outline delineates the microtremor survey (research) area used in this study.

highlight the combined influence of active faulting, complex basin geometry, and unconsolidated sediments on local site effects and surface damage. Recent studies have focused on geodiversity and geosite assessment in the Suoh aspiring geopark [10] and on the structural style and depositional history of the Semangko pull-apart basin [9]. Nevertheless, a systematic assessment of dynamic soil properties and seismic micro-zonation in Suoh remains lacking, despite its importance for sustainable development and disaster risk reduction in this tectonically active region.

Seismic micro-zonation commonly integrates geological, geomorphological, and geophysical data to delineate zones of different amplification potential [6]. Among available geophysical approaches, the Horizontal-to-Vertical Spectral Ratio (HVSR) method is widely used because it provides a rapid and cost-effective estimate of site resonance and amplification using ambient noise recordings [12]-[14]. Originally introduced by Nogoshi and Igarashi [15] and later popularized by Nakamura [16], HVSR uses the ratio between the horizontal and vertical components of ambient vibrations to estimate the fundamental resonance frequency (f_0) and amplification factor (A_0) of the soil column [12][17]-[22]. The combination of these parameters yields the seismic vulnerability index (K_g), which provides a simple indicator of the potential for damage to structures at a site [23]-[27]. Rather than reviewing the method exhaustively, it is noted here that HVSR has proven particularly useful in sedimentary basins where strong impedance contrasts exist between soft deposits and underlying bedrock [17][23][28]-[30]. Its advantages include low cost, ease of deployment, and the ability to operate in areas where strong-motion networks or detailed geotechnical data are limited.

In Sumatra, previous HVSR-based studies have

mainly focused on urban micro-zonation or regional -scale hazard assessment in the area [31]-[33]. While these studies provide valuable regional insights, they generally do not integrate HVSR derived parameters with inverted shear-wave velocity (V_s) models and 2D cross-sections to explicitly image basin geometry and engineering bedrock depth, particularly within pull-apart basin settings. As a result, small-scale lateral variations in site conditions within tectonic basins such as Suoh remain poorly resolved.

The novelty of this study lies in the combined use of HVSR-derived parameters, shallow V_s inversion, and 2D V_s cross-sections to characterize basin-scale heterogeneity and engineering bedrock geometry in the Suoh pull-apart basin. Shallow V_s models provide a physically interpretable link between HVSR parameters, sediment thickness, and site amplification, and are directly relevant to seismic hazard assessment and engineering applications. Previous studies in southern Sumatra have not yet combined this integrated framework with seismic micro-zonation in a pull-apart basin setting relevant to geopark development.

This study addresses these gaps by performing a detailed seismic micro-zonation of Suoh using HVSR and V_s inversion. Single-station microtremor measurements were conducted at 30 sites distributed across the basin. The data were processed to obtain f_0, A_0, and K_g, which were interpolated to generate spatial maps of dominant frequency, amplification factor, and seismic vulnerability. The HVSR curves were further inverted using the Dinver module of Geopsy to derive 1D V_s profiles at each site, constrained by the global CRUST1.0 crustal model and local

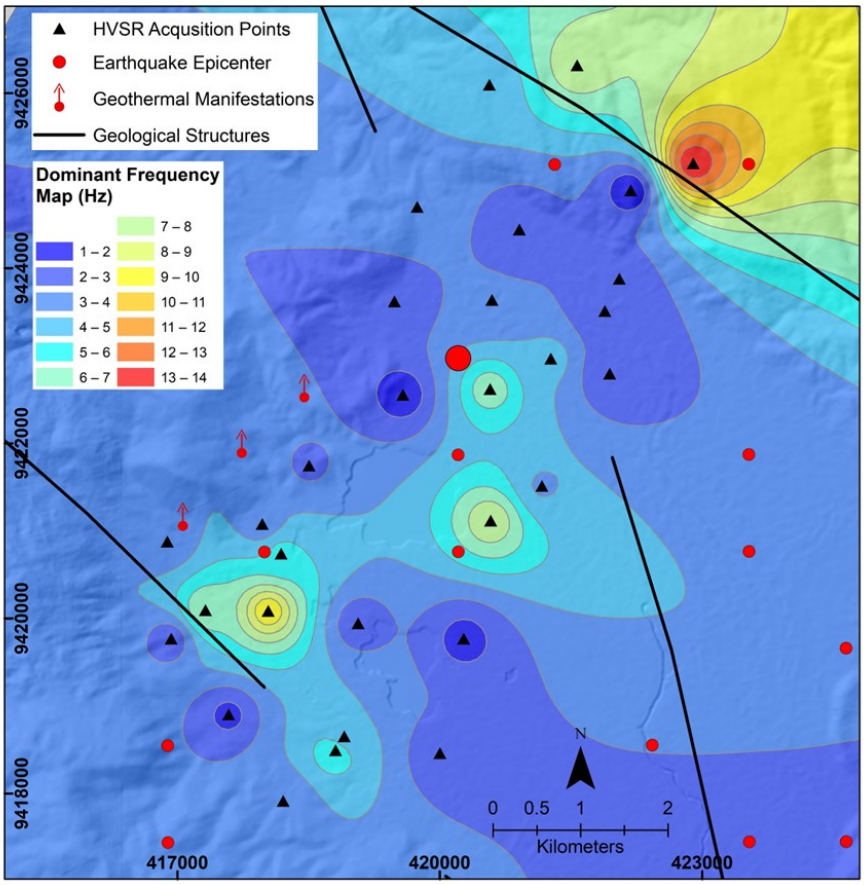

Figure 2. Dominant frequency (f_0) map derived from HVSR analysis in the Suoh area. Coloured shading and contour lines represent the interpolated dominant frequency values (in Hz). Black triangles show HVSR acquisition points, red circles indicate earthquake epicentres, red arrows mark geothermal manifestations, and black lines correspond to mapped geological structures (faults). Low-frequency zones (1–3 Hz) are concentrated in the central basin, whereas higher frequencies (>10 Hz) occur toward the northeastern margin on harder volcanic rocks.

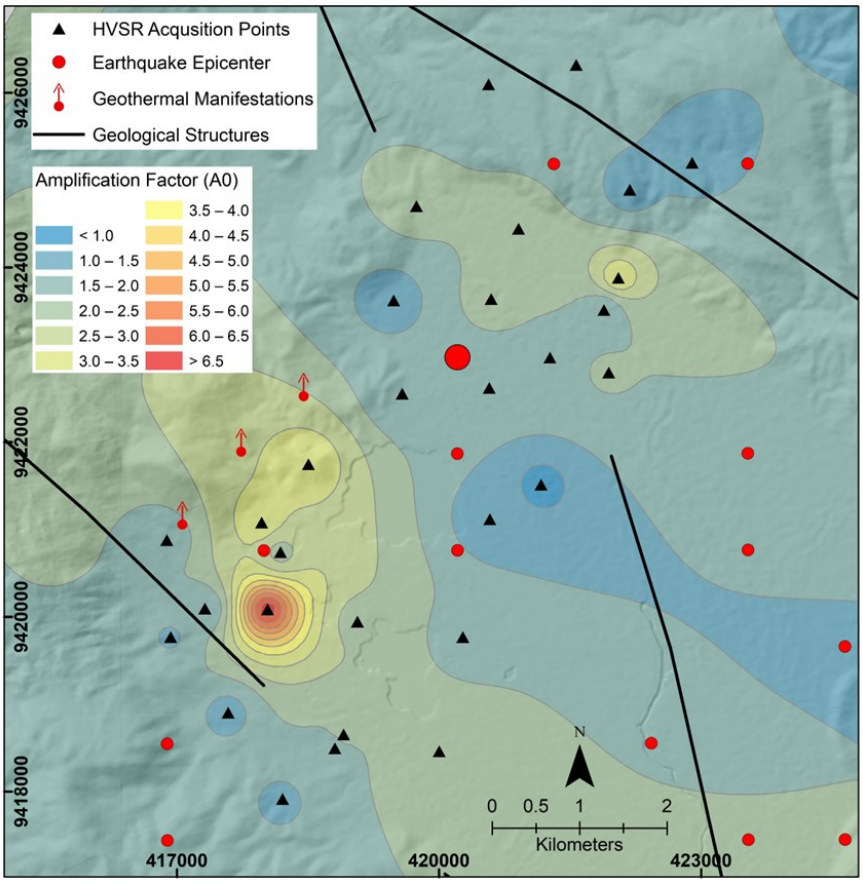

Figure 3. Amplification factor (A_0) map derived from HVSR analysis in the Suoh area. Coloured shading and contour lines represent the interpolated A_0 values. Black triangles indicate HVSR acquisition points, red circles show earthquake epicenters, red arrows mark geothermal manifestations, and black lines correspond to mapped geological structures (faults). The highest amplification factors ($A_0 > 4$) occur in the southwestern–central part of the basin, where thick-soft sediments overlie the active fault zone, whereas lower values ($A_o < 2$) dominate the eastern margin on competent volcanic rocks.

geological information. These profiles were combined into 2D V_s cross-sections along east–west and north–south profiles, revealing the 3D geometry of the basin fill and engineering bedrock. The HVSR and V_s-based microzonation is then compared with the distribution of shallow seismicity from the BMKG catalogue and with the main geological structures to assess how tectonics and sedimentary processes jointly control local site effects in Suoh.

The main objectives of this paper are therefore to: (i) characterize the spatial variation of HVSR-derived parameters (f_0, A_0, and K_g) in the Suoh pull-apart basin; (ii) infer the shallow V_s structure and engineering bedrock depth from HVSR inversion and 2D cross-sections; (iii) delineate seismic microzones and discuss their implications for hazard mitigation and spatial planning in Suoh.

2. MATERIALS AND METHODS

2.1. Materials

The primary dataset of this study consists of single-station microtremor recordings acquired at 30 sites distributed across the Suoh area, West Lampung, Indonesia (Figure 1). Each site was recorded for approximately 30 minutes with a sampling frequency of 100 Hz using three-component seismometers that measure two horizontal components (north–south and east–west) and one vertical component. The measurement sites were selected to represent the main lithological and morphological units in the study area while avoiding strong anthropogenic noise sources such as major roads, heavy machinery, and industrial facilities.

The instruments used were the Seismograf

Rakyat Indonesia (SRI) and Amadu portable seismometers. The SRI instrument is equipped with an ST-4.5B velocity sensor with a natural frequency of 4.5 Hz, while the Amadu sensors have a similar specification; both have sensitivities suitable for ambient-noise HVSR analysis. Field data were converted to miniSEED format and processed using the Geopsy software package to compute the horizontal-to-vertical spectral ratio (HVSR) curves at each site. The microtremor data were complemented by several auxiliary datasets, including a regional geological map at 1:250,000 scale, a digital elevation model (DEM) with 30 m resolution, administrative boundary maps, and the earthquake catalog provided by BMKG (1900–2024).

2.2. Methods

2.2.1. Microtremor Data Processing

The SRI and Amadu instruments are portable three-component seismometers with a flat response in the frequency range relevant for HVSR analysis (approximately 0.2–50 Hz). Both sensors have comparable natural periods and sensitivities suitable for ambient-noise measurements. Prior to analysis, records from both instruments were processed using an identical workflow in Geopsy, and no systematic amplitude bias was observed; therefore, no additional sensor-type correction was applied. At each site, 20–30 time windows were typically retained after visual inspection. Windows affected by transient anthropogenic noise or showing unstable spectral ratios were rejected following SESAME criteria.

Microtremor processing followed the recommendations of the SESAME guidelines [34] over the frequency range 0.2–20 Hz. For each site, the continuous record was divided into a series of time windows with lengths between 10 and 50 s. Window length was chosen so that it satisfied the SESAME requirement of being at least ten times the fundamental period and yielded a sufficient number of statistically independent windows. Before computing the Fourier spectra, each window was tapered with a Tukey window in order to reduce spectral leakage. Where distinct narrow-band noise unrelated to site response was observed (e.g., electrical or mechanical noise), a narrow Butterworth band-pass filter was applied. A Butterworth band-pass filter (0.2–20 Hz, fourth order) was applied only where narrow-band noise was present. This frequency range preserves the fundamental resonance peak while minimizing contamination from non-site related noise. The use of filtering was kept to a minimum so that the final HVSR curves remained representative of the true site response.

2.2.2. HVSR calculation

HVSR curves were computed from the Fourier amplitude spectra of the three components. For each window, the spectral amplitudes of the north–south (H_{NS}) and east–west (H_{EW}) horizontal components were combined using the root-mean-square (RMS), which was then divided by the vertical component spectrum (V). The HVSR function is defined as Equation (1).

$$HVSR = \sqrt{\frac{H_{NS}^2 + H_{EW}^2}{V^2}} \quad \textbf{(1)}$$

A representative HVSR curve for each site was obtained by averaging the individual-window curves, typically using the logarithmic median, and by computing confidence intervals that quantify the variability between windows. Curve quality was assessed on the basis of the stability of its shape across windows, the clarity of the main peak, and its consistency with the SESAME criteria [34].

2.2.3. Derivation of f_0, A_0, and Seismic Vulnerability Index (Kg)

Three key parameters were extracted from the HVSR curves at each site: the fundamental frequency (f_0), the amplification factor (A_0), and the seismic vulnerability index (K_g). The fundamental frequency f_0 was taken at the main HVSR peak and interpreted as the primary resonance frequency of the soil column. It depends on both the thickness and stiffness of the sediments overlying the bedrock. The amplification factor A_0 corresponds to the maximum HVSR amplitude at f_0 and reflects the degree of seismic-wave amplification caused by the impedance contrast between sediments and bedrock. Following previous work [14] and subsequent micro-zonation studies, the seismic vulnerability index is defined as Equation (2).

$$K_g = \frac{A_0^2}{f_0} \quad (2)$$

Larger K_g values indicate sites that are more susceptible to strong shaking, because they combine high amplification with resonance at periods that may coincide with the natural periods of buildings. In this study, K_g was classified into three classes: low vulnerability (K_g < 1.5), moderate vulnerability (1.5 ≤ K_g ≤ 2.5), and high vulnerability (K_g > 2.5).

2.2.4. Spatial Interpolation and Seismic Microzonation

The values of f_0, A_0, and K_g obtained at the 30 sites were interpolated onto a regular grid using Kriging. This procedure produced contour maps of fundamental frequency, amplification factor, and seismic vulnerability over the Suoh area, capturing the lateral variability of site response. The interpolated K_g map, after reclassification into low, moderate, and high vulnerability classes, was interpreted together with geological maps, topography, and local seismicity patterns. This integrated analysis was used to delineate seismic microzones and to provide a basis for mitigation strategies and land-use planning in Suoh.

2.2.5. 1D Inversion of HVSR Curves for Vs Models

The HVSR curves at each site were further inverted to retrieve one-dimensional shear-wave velocity (V_s) profiles. The inversion was carried out using the Dinver module in the Geopsy package, which computes theoretical HVSR curves for layered 1D models and compares them with the observed curves. At each site, the subsurface was

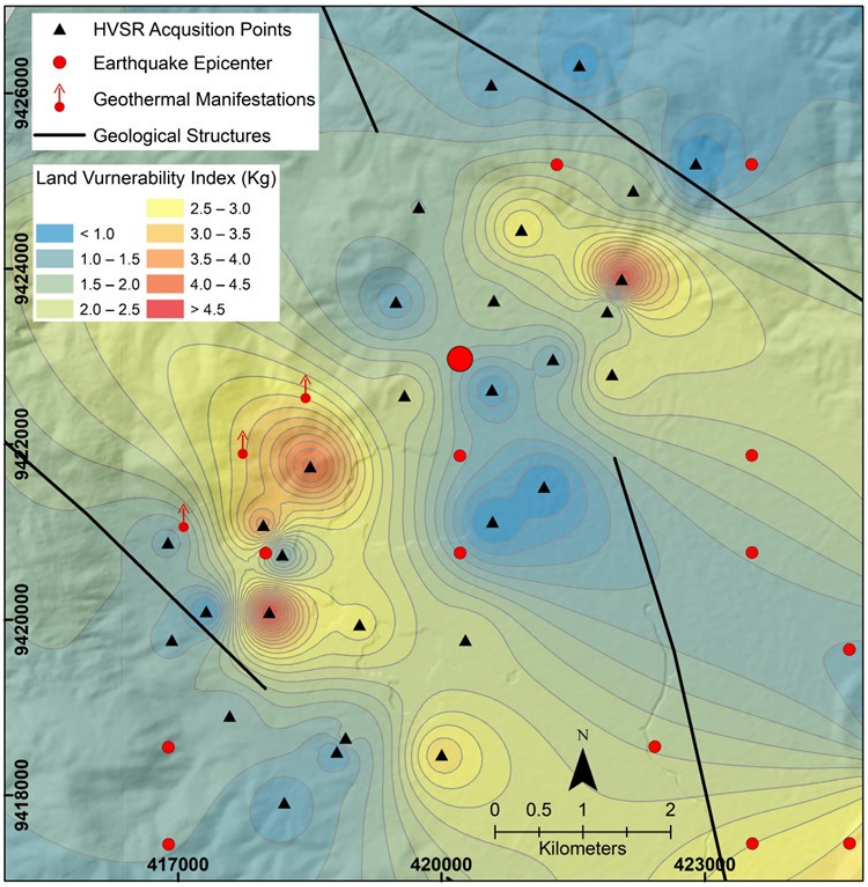

Figure 4. Land vulnerability index (K_g) map of the Suoh area derived from HVSR analysis. Coloured shading and contour lines represent the interpolated K_g values, classified into seven vulnerability classes. Black triangles indicate HVSR acquisition points, red circles show earthquake epicenters, red arrows mark geothermal manifestations, and black lines correspond to mapped geological structures (faults). Zones with high K_g (> 4.5) are concentrated in the central–western part of the basin, where thick-soft sediments and active structures coincide, indicating the highest expected seismic site amplification and land vulnerability.

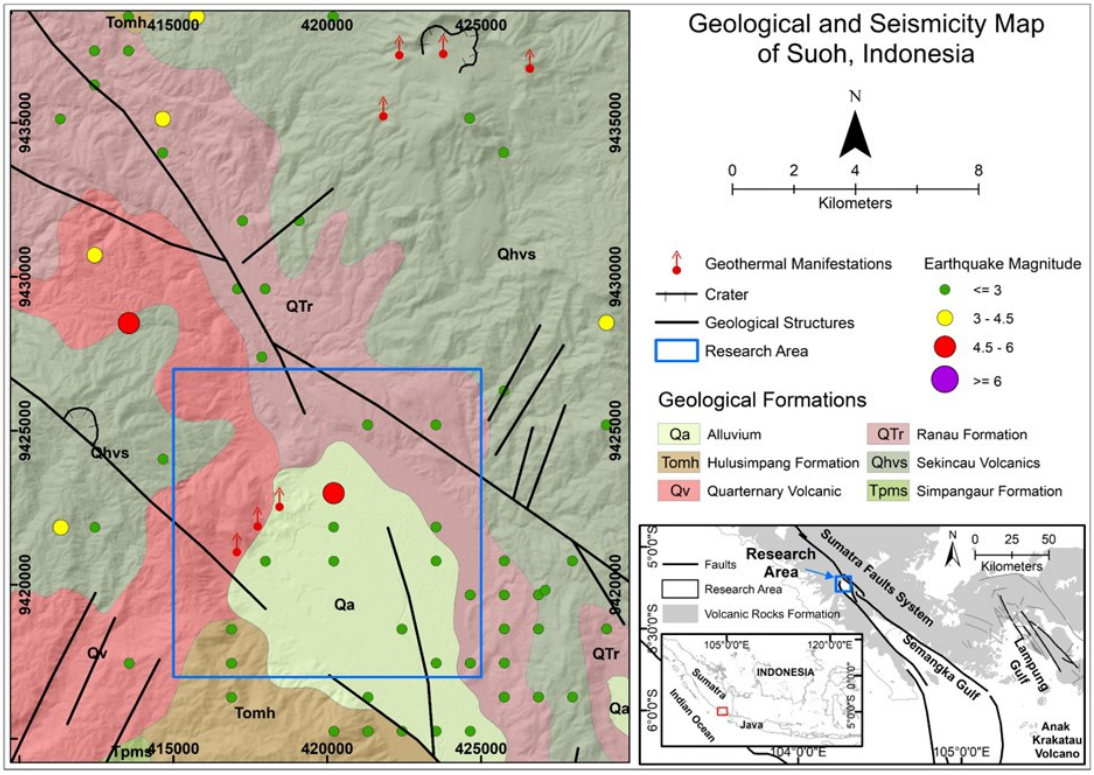

Figure 5. Geological and seismicity map of the Suoh area, southern Sumatra. The coloured polygons show the main geological formations (Qa = Alluvium, Tomh = Hulusimpang Formation, Qv = Quaternary Volcanic, QTr = Ranau Formation, Qhvs = Sekincau Volcanics, Tpms = Simpangaur Formation). Green–yellow–red–purple circles represent earthquake epicentres classified by magnitude, red arrows indicate geothermal manifestations, black lines correspond to mapped geological structures (faults), and the blue rectangle outlines the microtremor (HVSR) research area. The inset map (lower right) locates the study area along the Sumatra Fault System in southern Sumatra, Indonesia [37].

parameterized as a stack of 4–5 sediment layers overlying a half-space bedrock. The unknown parameters were layer thickness (H), shear-wave velocity (V_s), compressional-wave velocity (V_p), and density (ρ). The initial model and parameter bounds were derived from the global crustal model CRUST1.0 [35] for the cell covering the Suoh region, and then adjusted using local geological information so that V_s values in the shallow sediments and in the engineering bedrock remained realistic. Although CRUST1.0 has a coarse spatial resolution, it was used only as a first-order constraint to define reasonable parameter bounds for deep layers. Shallow sediment properties were primarily constrained by HVSR data and local geology, thereby minimizing the influence of the global model on basin-scale features. Dinver explores the model space non-linearly and minimizes the misfit between observed and theoretical HVSR curves in logarithmic amplitude over the 0.2–20 Hz band. Model acceptance was based on the logarithmic misfit between observed and synthetic HVSR curves. Models with misfit values within the lowest 10–15% of the total population were considered acceptable. The best-fit model corresponds to the minimum misfit while remaining consistent with surface geology and lateral continuity between neighboring sites. For each site, a set of acceptable models is obtained; from this ensemble, a best-fit model is selected as the one with the lowest misfit that is also consistent with surface geology and with the spatial trend of V_s at neighboring sites. These 1D V_s profiles form the basis for constructing the 2D velocity section.

3. RESULTS AND DISCUSSIONS

3.1. Dominant Frequency (f_0)

The contour map of f_0 (Figure 2) shows values

ranging from 0.5 to 14.5 Hz. Low frequencies (0.5–3 Hz) are concentrated in the western and central parts of Suoh, whereas high frequencies (>10 Hz) occur in the northeastern area. Low f_0 values indicate thick, unconsolidated sedimentary layers that can trap seismic energy for a longer time and generate long-period ground motion. In contrast, the northeastern area with high f_0 (≥10 Hz) is dominated by hard rock with thin sediment cover, which is more stable from a seismic point of view. According to the Kanai soil classification [36], zones with low f_0 belong to soil classes III–IV, corresponding to sediment thicknesses greater than 30 m and a high potential for resonance during earthquakes.

In general, f_0 reflects both the thickness of the sedimentary layers and the type of underlying bedrock. The relationship between sediment thickness (h) and shear-wave velocity (V_s) with the dominant frequency can be expressed by $f_0 \propto V_s/4h$. Low f_0 values therefore point to thick, soft sediments that can significantly amplify ground shaking, whereas high f_0 is associated with hard rocks with large impedance, which tend to reduce amplification. Low frequencies (≤1 Hz) are mainly observed in the central Suoh basin, which is dominated by thick alluvial deposits and loose volcanic material, while high frequencies (≥10 Hz) are found over the surrounding hills near Mount Sekincau and Mount Seminung, where andesitic lava flows and volcanic breccias crop out. The spatial pattern of f_0 is therefore consistent with the tectonic–sedimentary setting of a pull-apart basin: the centre of the basin acts as a sediment trap with thick low-velocity deposits and low resonance frequency, whereas the margins are formed by volcanic highs with thin, stiff cover. This contrast controls the expected dominant period of shaking across Suoh.

3.2. Amplification Factor (A_0)

The contour map of A_0 (Figure 3) indicates values between 0.6 and 6.6. High amplification (≥4) is concentrated in the southwestern to central parts of the study area. These high A_0 values reflect strong seismic-wave amplification caused by a large impedance contrast between the soft surface sediments and the underlying stiffer bedrock. Most of the shallow seismic activity is distributed around the areas with high A_0, especially in the western and central zones, which also coincide with low-f_0 areas. This positive correlation suggests that zones with thick, low-velocity sediments tend to experience both stronger amplification and more intense seismicity.

Physically, amplification occurs when seismic waves propagate from stiff bedrock into softer near-surface layers. As the wave speed decreases, the amplitude increases and energy becomes trapped in the shallow medium. In Suoh, this effect is enhanced by the presence of tuff, volcanic sand, and clay in the central basin, which promote resonance. The amplification map (Figure 3) shows that areas with $A_0 > 3$ correspond to alluvial deposits and tuff derived from the activity of Mount Sekincau, accumulated above the northwest–southeast oriented active fault segments. In the eastern area, where A_0 is low (≤2), the near-surface rocks are denser and more competent, so the potential for amplification is relatively small.

3.3. Seismic Vulnerability Index (K_g)

The seismic vulnerability index K_g (Figure 4), obtained from the combination of A_0 and f_0, ranges from about –0.2 to 4.8. High values (>2.5) are distributed mainly in the western and central parts of Suoh, indicating a high level of vulnerability to strong ground shaking. The dense seismic activity in these zones confirms that areas with thick, low-impedance sediments are prone to strong amplification of seismic waves. In contrast, the eastern part of Suoh shows low K_g values (<1) and sparse seismicity, reflecting more stable geological conditions. Following the classification in previous work [14], zones with $K_g > 2$ fall into the medium-to-high vulnerability category and should be prioritized in seismic mitigation and infrastructure planning.

Based on the K_g distribution, the study area can be divided into three main vulnerability zones: Low vulnerability ($K_g < 1.5$), located in the northern and western parts of Suoh, composed mainly of andesitic–basaltic volcanic rocks and breccias. Moderate vulnerability ($1.5 \leq K_g \leq 2.5$), scattered in the southwestern to southern area, with mixed lithology of volcanic rocks and colluvial deposits. High vulnerability ($K_g > 2.5$) – are concentrated in the central–western part of the basin, where thick

sediment layers (>30 m) with high amplification potential are inferred. The HVSR method is thus able to identify significant variations in dominant frequency and seismic vulnerability index across the Suoh basin, which directly affect the level of ground-motion amplification and the potential for infrastructure damage. The presence of thick fluvio –volcanic deposits overlying hard bedrock implies that these areas are susceptible to low-frequency ground resonance, typically associated with strong shaking during large earthquakes. The resulting micro-zonation map displays zones of high amplification in the central and southeastern basin, aligned with the active segment of the Sumatra Fault Zone (SFZ).

3.4. Seismic Microzonation of the Suoh Area

Integration of the three HVSR-derived parameters (f_0, A_0, and K_g) yields a seismic microzonation map for Suoh that can be divided into three main zones: (1) Low vulnerability zone, located in the eastern to northeastern part of the study area, this zone is dominated by hard volcanic rocks and breccias, with high f_0 (>10 Hz) and low A_0 (<2). It is relatively stable and suitable for basic infrastructure development; (2) Moderate vulnerability zone, found in the southern and southwestern parts, this zone is characterized by f_0 values of 3–8 Hz and A_0 of 2–4. It represents a transition between hard rock and soft sediments. Development is still possible here, but structures should be designed with adequate earthquake-resistant provisions; (3) High vulnerability zone, extending across the western to central Suoh area, this zone is associated with thick sedimentary layers (f_0 < 2 Hz) and high amplification ($A_0 \geq 4$). It is expected to experience the strongest shaking during earthquakes due to combined resonance and low impedance conditions.

The correlation between the micro-zonation map and the distribution of seismicity indicates that the western–central Suoh region is the most vulnerable, as it exhibits both high K_g values and dense shallow earthquake activity. This pattern is parallel to the NW–SE trend of the Semangko Fault, which controls deformation and sediment deposition within the basin. The seismic micro-zonation, therefore, captures both the geological and tectonic controls on local site effects and provides a robust basis for risk-informed land-use planning.

3.5. Seismicity Pattern and Geological Correlation

Seismicity analysis using the BMKG catalogue for the period 1900–2024 shows that Suoh and its

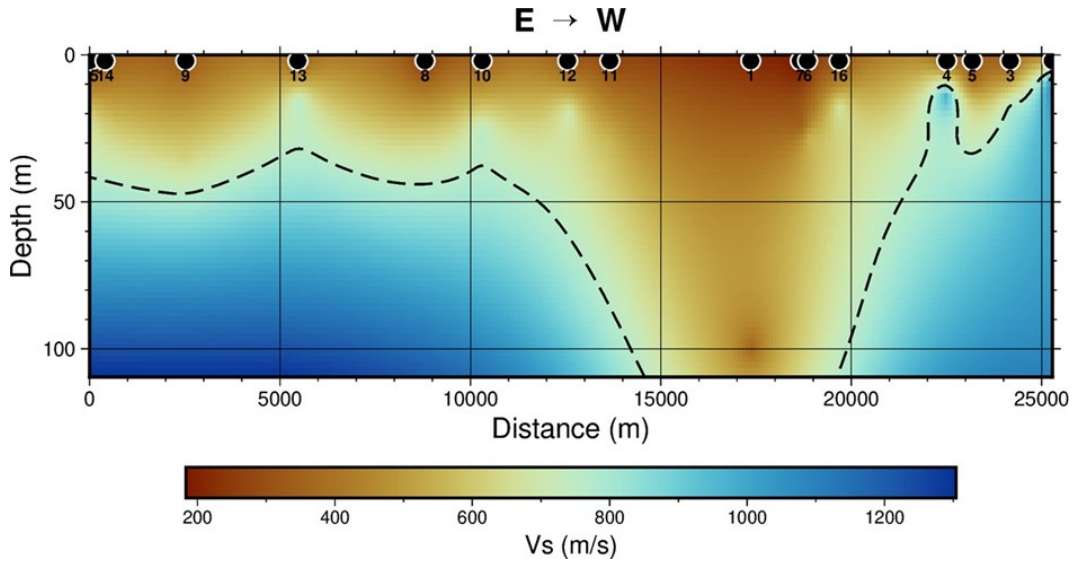

Figure 6. East–west 2D shear-wave velocity section across the Suoh basin. Colours represent shear-wave velocity V_s (m/s), with warm colours indicating low velocities (soft sediments) and cool colours indicating high velocities (stiff material). Black circles at the surface denote the locations of the HVSR sites (station IDs are labelled). The dashed black line marks the approximate depth to the engineering bedrock, defined here by $V_s \approx$ 760-800 m/s. Note the deepening of the low-V_s basin in the central part of the profile (distances ~10–15 km), where thick soft sediments overlie the basement.

surroundings have experienced earthquakes with magnitudes between 1.4 and 6.9 and focal depths from 1 to 198 km (Figure 5). The catalogue was clipped to a radius of about 10 km around the centre of the Suoh basin to capture the local tectonic response controlled by the Semangko segment of the Sumatra Fault. Vertically, the earthquakes can be grouped into two main depth ranges: shallow events at depths <30 km and intermediate–deep events at depths >70 km. The former represents upper-crustal faulting directly associated with the Semangko segment, while the latter are related to the Benioff zone of the subducting Indo-Australian Plate.

The Suoh Basin is also characterized by geothermal manifestations (maars, craters, and lava domes) associated with ongoing volcanism. Although volcanic earthquakes differ in mechanism from tectonic ones, the presence of this volcanic system often correlates with zones of shallow earthquake foci triggered by changes in fluids and stress within the crust. The Semangko Fault and its secondary faults in the Suoh Basin create zones of weakness in the Earth's crust. These zones serve as pathways for energy movement and stress concentration, causing earthquakes to occur more frequently along the main fault structures and their associated substructures. The seismicity pattern in this basin is strongly controlled by regional geological structures, particularly the active segments of the Great Sumatran Fault and the pull-apart basin features formed as a result of the transtensional tectonic regime. Active faults cause stress concentration, making earthquakes frequent along these structures. The basin structure and volcanic manifestations also influence the distribution of intermediate and shallow earthquakes in the study area. Overall, the earthquake pattern is not random but directly correlates with the controlling geological structures.

For microzonation and local site-effect assessment, the shallow earthquakes are the most relevant because they generate higher peak ground accelerations and are more sensitive to near-surface sediment conditions. Spatially, shallow epicenters show an elongated NW–SE pattern that follows the trace of the Semangko Fault and the structural boundaries of the Suoh basin. The most prominent seismicity cluster lies in the western–central basin, coincident with zones of low f_0 and high K_g identified from HVSR analysis. This correlation suggests that the area is not only located above an active fault, but is also covered by thick, soft sediments that can strongly amplify shaking. In contrast, the eastern–northeastern sector, dominated by hard volcanic rocks, has lower epicentral density and mainly belongs to the low-to-moderate vulnerability classes. Overlaying the seismicity map with the vulnerability index (Figure 4) confirms a spatial match between tectonically active zones and areas with medium-to-high K_g. This implies a "double" seismic risk in Suoh: the areas that accumulate the largest tectonic stress are simultaneously those with the most unfavourable dynamic soil properties. Similar patterns have been reported in other tectono–volcanic basins, where the combination of thick, soft sediments and proximity to active faults is a key factor in increasing the potential for damage to infrastructure.

3.6. Shear-wave Velocity Structure from 2D Cross-sections

The 2D V_s sections along the east–west (E–W) and north–south (N–S) profiles (Figures 6 and 7) provide additional constraints on the subsurface structure inferred from the HVSR analysis. Both profiles clearly display a strong contrast between low-velocity sediments in the interior of the Suoh basin and higher-velocity units toward the surrounding volcanic highs. Near the surface, layers with V_s < 400 m/s extend down to depths of approximately 20–40 m over large parts of the profiles, especially in their central segments. These low velocities are interpreted as unconsolidated alluvial and volcanic deposits, consistent with the geological mapping and with the high A_0 and K_g values obtained in the same areas.

In the E–W profile (Figure 6), the engineering bedrock is consistently defined as layers with shear-wave velocity $V_s \geq 800$ m/s, whereas layers with $V_s \approx$ 760-800 m/s (indicated by the dashed line) are interpreted as transitional due to inversion uncertainty. The engineering bedrock is relatively shallow (< 40 m) at the eastern and western ends of the section but deepens to more than 80–100 m between about 10 and 15 km along the profile. This central deepening coincides with the low-f_0 (0.5–2 Hz) and high-K_g zones mapped in the middle of the

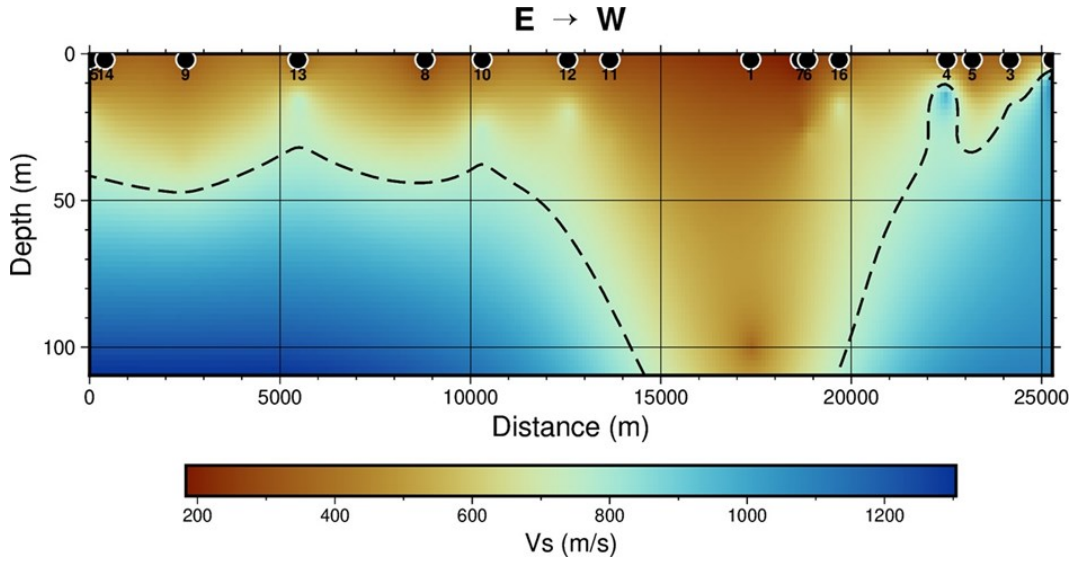

Figure 7. North–south 2D shear-wave velocity section based on the same set of inverted 1D V_s models. The dashed line again indicates the approximate engineering bedrock depth ($V_s \approx$ 760-800 m/s). The section shows an asymmetric basin geometry, with thicker low-V_s sediments (< 400 m/s) in the southern part of the profile and a shallower basement toward the north.

basin, confirming that the thickest sedimentary infill is located above the pull-apart depocenter. The resulting geometry is typical of tectono-sedimentary basins along strike-slip faults, where transtensional deformation creates localized subsidence and enhanced sediment accumulation.

The N–S profile (Figure 7) reveals a similar but slightly asymmetric pattern. The basement is relatively shallow beneath the northern part of the profile, whereas to the south it dips to depths exceeding 60–80 m and is overlain by a thick wedge of low-velocity sediments. This southern thickening matches the area where moderate-to-high K_g values and clusters of shallow seismicity are observed. The combination of thicker-soft sediments and proximity to the active Semangko segment implies that this sector is particularly prone to strong site amplification. Taken together, the two cross-sections show that the amplification pattern in Suoh is controlled not only by vertical impedance contrasts but also by the 3D geometry of the basin. Zones where the engineering bedrock is deepest correspond systematically to low f_0, high A_0, and high K_g, in agreement with previous HVSR-based studies in sedimentary and volcanic basins (e.g., [34][38]). This reinforces the conclusion that the central parts of the Suoh pull-apart basin represent the most critical areas in terms of local site effects and should be prioritised in seismic risk mitigation and land-use planning.

The 2D shear-wave velocity V_s cross-sections derived from inverted HVSR models (Figures 6 and 7) reveal a basin geometry characterized by low-velocity sedimentary fills overlying higher-velocity basement units. This geometry is broadly consistent with previously published geological cross-sections of the Suoh–Semangko pull-apart basin, which describe thick accumulations of fluvio-volcanic and lacustrine sediments bounded by volcanic and basement rocks along the basin margins [7][9]. In particular, the deepening of the engineering bedrock toward the basin center inferred from the V_s sections align with geological interpretations of localized subsidence associated with trans-tensional deformation along the Semangko Fault.

Direct validation using borehole or deep drilling data is currently not available in the study area; therefore, the V_s derived basin geometry should be interpreted as a first-order approximation. Nevertheless, the depth trends inferred from the HVSR inversion are supported indirectly by surface geological mapping, stratigraphic relationships, and the spatial distribution of low dominant frequencies (f_0) obtained in this study. Similar levels of agreement between HVSR-based V_s models and geological cross-sections have been reported in other tectonically active sedimentary basins lacking borehole control. Consequently, the integrated

interpretation of HVSR parameters and 2D V_s imaging provides a reasonable representation of the subsurface structure of the Suoh basin, while highlighting the need for future validation using borehole or active-source seismic data.

3.7. Implications for Hazard Mitigation, Land Use, and the Suoh Aspiring Geopark

The combined HVSR parameters (f_0, A_0, K_g) and 2D V_s cross-sections clearly show that the Suoh pull-apart basin is characterised by strong lateral contrasts in local site conditions. Areas where the engineering bedrock is deepest and V_s remains below about 400 m/s over several tens of metres coincide with low dominant frequencies (0.5–2 Hz), large amplification factors ($A_0 \geq 3$), and high seismic vulnerability indices ($K_g > 2.5$). These zones, mainly in the central and western parts of the basin, represent the most critical areas in terms of expected ground shaking. In contrast, the eastern and northeastern margins, where bedrock is shallow and $K_g < 1.5$, can be considered relatively stable from a site-effect perspective.

From a practical viewpoint, the micro-zonation maps provide preliminary, quantitative information that may support risk-informed spatial planning in Suoh. Rather than prescribing specific land-use decisions, the vulnerability classes identified in this study are intended to complement existing regional spatial plans and Indonesian building codes. Areas characterized by higher seismic vulnerability (high-K_g) may warrant greater attention in future detailed geotechnical investigations, while areas underlain by competent rock (low-K_g) are comparatively more suitable for infrastructure development when considering local site effects. In moderate-vulnerability zones, new construction remains feasible provided that building designs account for local resonance frequencies and expected amplification, in accordance with national seismic design standards and microzonation-based approaches [6][12][13].

The results also emphasise the need to integrate geological, geomorphological, and seismological information when planning geopark development in tectonically active regions. In Suoh, the most attractive geosites linked to the Semangko Fault, volcanic centres, and pull-apart basin morphology often coincide with high-K_g zones. Careful zoning is therefore required so that geotourism infrastructure is located in safer areas while high-risk zones are maintained as observation points or restricted access sites with appropriate safety measures. This approach is consistent with recent geo-hazard-oriented geopark management studies, which stress that geoconservation and disaster risk reduction must be addressed simultaneously in geopark planning [14][28][29].

Finally, although the present micro-zonation already provides valuable guidance for local authorities, it should be regarded as a first-order model. Future work should refine the zoning by integrating additional geotechnical boreholes, MASW or SPAC surveys, and strong-motion simulations for scenario earthquakes on the Semangko segment. Such an integrated framework will improve the robustness of hazard estimates and help transform Suoh into a resilient geopark that balances geotourism development, environmental conservation, and seismic risk management.

4. CONCLUSIONS

This study demonstrates that integrating HVSR analysis with shear-wave velocity inversion provides an effective framework for seismic micro-zonation in the Suoh pull-apart basin. HVSR-derived parameters reveal strong lateral variations in dominant frequency, amplification, and seismic vulnerability, with low-frequency, high-vulnerability zones concentrated in the central–western basin where thick-soft sediments overlie deep engineering bedrock ($V_s \geq 800$ m/s). The 2D V_s cross-sections confirm a deep low-velocity depocentre consistent with pull-apart basin tectonics and correlated with clustered shallow seismicity along the Semangko Fault. These results highlight the critical role of basin geometry in controlling local site effects and offer a practical basis for risk-informed spatial planning in Suoh. However, the main limitation of this study is that the subsurface model is derived solely from HVSR inversion of ambient-noise data, which is inherently non-unique and cannot fully resolve velocity–thickness trade-offs without independent constraints. Therefore, the presented micro-zonation should be regarded as a first-order approximation that would benefit from future validation and

refinement using borehole data, active-source seismic methods (e.g., MASW or SPAC), and strong-motion observations to improve the robustness of seismic hazard assessment.

AUTHOR INFORMATION

Corresponding Author

Rahmi Mulyasari — Department of Geological Engineering, Lampung University, Bandar Lampung-35145 (Indonesia);
orcid.org/0000-0003-2723-5750
Email: rahmi.mulyasari@eng.unila.ac.id

Authors

Muh. Sarkowi — Department of Geophysical Engineering, Lampung University, Bandar Lampung-35145 (Indonesia);
orcid.org/0000-0001-8554-3407

Nandi Haerudin — Department of Geophysical Engineering, Lampung University, Bandar Lampung-35145 (Indonesia);
orcid.org/0000-0002-2800-4172

Hari Wiki Utama — Department of Geological Engineering, Jambi University, Muaro Jambi-35361 (Indonesia);
orcid.org/0000-0001-6890-3730

Angga Jati Widiatama — Department of Geological Engineering, Institute of Technology Sumatra, South Lampung-35365 (Indonesia);
orcid.org/0000-0002-7960-0046

I Gede Boy Darmawan — Department of Geological Engineering, Lampung University, Bandar Lampung-35145 (Indonesia);
orcid.org/0000-0002-6368-4070

Andri Kurniawan — Department of Geophysical Engineering, Lampung University, Bandar Lampung-35145 (Indonesia);
orcid.org/0009-0001-0761-7674

Yayan Mi'rojul Husni — Department of Geophysical Engineering, Lampung University, Bandar Lampung-35145 (Indonesia);
orcid.org/0009-0002-6958-2451

Hesti Hesti — Department of Geological Engineering, Lampung University, Bandar Lampung-35145 (Indonesia);
orcid.org/0009-0006-6448-7585

Nofita Fatmawati — Department of Geophysical Engineering, Lampung University, Bandar Lampung-35145 (Indonesia);
orcid.org/0009-0000-0977-2574

Serli Marlina — Department of Geophysical Engineering, Lampung University, Bandar Lampung-35145 (Indonesia);
orcid.org/0009-0002-4205-3808

Author Contributions

Conceptualization, R. M. and M. S.; Methodology, and Supervision, N. H. and H. W. U.; Software, I. G. B. D. and Y. M. H.; Validation, A. J. W. and A. K.; Formal Analysis, N. F. and S. M.; Investigation, M. S. and H. H.; Resources, Writing – Original Draft Preparation, and Writing – Review & Editing, R. M. and A. K.; Visualization, I. G. B. D. and Y. M. H.

Conflicts of Interest

The authors declare no conflict of interest.

ACKNOWLEDGEMENT

This research was supported by the Ministry of Education, Research, and Technology (KEMENDIKBUDRISTEK) through Regular Fundamental Research (Contract Number: 057/E5/PG.02.00.PL/2024). The authors would like to express their gratitude to the Institute for Research and Community Service (LPPM), University of Lampung (Unila), for their administrative support. The authors also thank the West Lampung Government for the support given to the research.

DECLARATION OF GENERATIVE AI

During the preparation of this work, the author(s) used QuillBot (https://quillbot.com) to translate portions of the manuscript from Indonesian to English, and used ChatGPT (for drafting, polishing language, and generating wording suggestions). After using these tools, the author(s) reviewed and edited the content as needed and take full responsibility for the content of the publication.

REFERENCES

[1] S. Bonnefoy-Claudet, F. Cotton, and P. Y. Bard. (2006). "The Nature Of Noise Wavefield And Its Applications For Site

Effects Studies: A Literature Review". *Earth-Science Reviews.* **79** (3-4). 10.1016/j.earscirev.2006.07.004.

[2] S. Molnar, A. Sirohey, J. Assaf, P. Bard, S. Castellaro, C. Cornou, B. Cox, B. Guillier, B. Hassani, H. Kawase, S. Matsushima, F. J. Sanchez-Sesma, and A. Yong. (2022). "A Review Of The Microtremor Horizontal-To-Vertical Spectral Ratio (MHVSR) Method". *Journal of Seismology.* **26** (4). 10.1007/s10950-021-10062-9.

[3] A. M. Lontsi, M. Hobiger, F. Panzera, F. J. Sanchez-Sesma, and D. Fah. (2023). "Seismic Characterization Of Swiss Strong Motion Borehole Station Sites By Inversion Of Full Microtremor Horizontal To Vertical Spectral Ratios H V(z,f)". *Bulletin of the Seismological Society of America.* **113** (1). 10.1785/0120210320.

[4] H. Sharma, S. Molnar, and A. Sirohey. (2024). "Techniques To Identify Microtremor Wave Contributions And Impact To Seismic Site Characterization". *Journal of Seismology.* **28** (2). 10.1007/s10950-024-10189-5.

[5] S. Molnar, J. Assaf, A. Sirohey, and S. R. Adhikari. (2020). "Overview Of Local Site Effects And Seismic Microzonation Mapping In Metropolitan Vancouver British Columbia Canada". *Engineering Geology.* **270** : 105568. 10.1016/j.enggeo.2020.105568.

[6] N. Chieffo and A. Formisano. (2019). "Geo Hazard Based Approach For The Estimation Of Seismic Vulnerability And Damage Scenarios Of The Old City Of Senerchia Avellino Italy". *Geosciences.* **9** (2): 59. 10.3390/geosciences9020059.

[7] K. Sieh and D. Natawidjaja. (2000). "Neotectonics Of The Sumatran Fault Indonesia". *Journal of Geophysical Research: Solid Earth.* **105** (B12). 10.1029/2000JB900120.

[8] A. F. Putra and S. Husein. (2016). "Pull Apart Basins Of Sumatran Fault: Previous Works And Current Perspectives Regional Setting Pull Apart Basin Along".

[9] M. M. Mukti. (2018). "Structural Style And Depositional History Of The Semangko Pull Apart Basin In The Southeastern Segment Of Sumatra Fault Zone". *Riset Geologi dan Pertambangan.* **28** (1). 10.14203/risetgeotam2018.v28.954.

[10] D. Muslim, Z. Zakaria, H. Rachmat, P. Iqbal, G. O. Muslim, M. S. Sadewo, and F. N. Muslim. (2022). "Identification Of Geodiversity And Geosite Assessment Around Geohazard Area Of Suoh Aspiring Geopark In West Lampung Sumatra Indonesia". *Resources.* **11** (11): 104. 10.3390/resources11110104.

[11] M. Sarkowi, R. C. Wibowo, and S. Ida Bagus. (2022). "Potensi Gempabumi Di Sepanjang Sesar Semangko Segmen Lampung". *Jurnal Teknik Infrastruktur dan Teknologi Informasi.* **3** (2). 10.23960/jtii.v3i2.50.

[12] R. Xu and L. Wang. (2021). "The Horizontal To Vertical Spectral Ratio And Its Applications". *EURASIP Journal on Advances in Signal Processing.* **2021** (1). 10.1186/s13634-021-00765-z.

[13] J. P. Vantassel, A. C. Stolte, L. M. Wotherspoon, and B. R. Cox. (2023). "AutoHVSR: A Machine Learning Supported Algorithm For The Fully Automated Processing Of Horizontal To Vertical Spectral Ratio Measurements". *Soil Dynamics and Earthquake Engineering.* **173** : 108153. 10.1016/j.soildyn.2023.108153.

[14] Y. Nakamura. (2000). "Clear Identification Of Fundamental Idea Of Nakamura's Technique And Its Applications".

[15] M. Nogoshi and T. Igarashi. (1971). "On The Amplitude Characteristics Of Microtremor Part 2". *Zisin: Journal of the Seismological Society of Japan Second Series.* **24** (1). 10.4294/zisin1948.24.1_26.

[16] Y. Nakamura. (1989). "Method For Dynamic Characteristics Estimation Of Subsurface Using Microtremor On The Ground Surface". *Quarterly Report of the Railway Technical Research Institute.* **30** (1).

[17] M. Rong, L. Fu, and J. X. Wang. (2020). "On The Differences Between Horizontal-To-Vertical Spectral Ratios Caused By Earthquakes And Ambient Noise: A Case Study Of Vertical-Array Observations In

Northern China". *Journal of Applied Geophysics.* **182** : 104171. 10.1016/j.jappgeo.2020.104171.

[18] S. Y. Kang, K. H. Kim, J. M. Chiu, and L. Liu. (2020). "Microtremor HVSR Analysis Of Heterogeneous Shallow Sedimentary Structures At Pohang South Korea". *Journal of Geophysics and Engineering.* **17** (5). 10.1093/jge/gxaa035.

[19] L. Agostini, J. Boaga, A. Galgaro, and A. Ninfo. (2015). "HVSR Technique In Near-Surface Thermal-Basin Characterization: The Example Of The Caldiero District North-East Italy". *Environmental Earth Sciences.* **74** (2). 10.1007/s12665-015-4109-0.

[20] S. Maghami, A. Sohrabi-Bidar, S. Bignardi, A. Zarean, and M. Kamalian. (2021). "Extracting The Shear Wave Velocity Structure Of Deep Alluviums Of Qom Basin Iran Employing HVSR Inversion Of Microtremor Recordings". *Journal of Applied Geophysics.* **185** : 104246. 10.1016/j.jappgeo.2020.104246.

[21] T. Ornthammarath, A. Jirasakjamroonsri, P. Pornsopin, R. Rupakhety, N. Poovarodom, P. Warnitchai, and T. T. T. Toe. (2023). "Preliminary Analysis Of Amplified Ground Motion In Bangkok Basin Using HVSR Curves From Recent Moderate To Large Earthquakes". *Geoenvironmental Disasters.* **10** (1). 10.1186/s40677-023-00259-0.

[22] C. T. Chen, K. L. Wen, and J. Y. Huang. (2020). "Source Location Dependency Site Response In The Taipei Basin Of Taiwan By Using HVSR Analysis". *Journal of Asian Earth Sciences.* **191** : 104223. 10.1016/j.jseaes.2019.104223.

[23] I. Khadrouf, O. El Hammoumi, N. El Goumi, and M. Oukassou. (2024). "Contribution Of HVSR MASW And Geotechnical Investigations In Seismic Microzonation For Safe Urban Extension: A Case Study In Ghabt Admin Agadir Western Morocco". *Journal of African Earth Sciences.* **210** : 105138. 10.1016/j.jafrearsci.2023.105138.

[24] A. H. Farazi, M. S. Hossain, Y. Ito, J. Pina-Flores, A. S. M. M. Kamal, and M. Z. Rahman. (2023). "Shear Wave Velocity Estimation In The Bengal Basin Bangladesh By HVSR Analysis: Implications For Engineering Bedrock Depth". *Journal of Applied Geophysics.* **211** : 104967. 10.1016/j.jappgeo.2023.104967.

[25] P. Capizzi and R. Martorana. (2022). "Analysis Of HVSR Data Using A Modified Centroid-Based Algorithm For Near-Surface Geological Reconstruction". *Geosciences.* **12** (4): 147. 10.3390/geosciences12040147.

[26] M. Tun, E. Pekkan, O. Ozel, and Y. Guney. (2016). "An Investigation Into The Bedrock Depth In The Eskisehir Quaternary Basin Turkey Using The Microtremor Method". *Geophysical Journal International.* **207** (1). 10.1093/gji/ggw294.

[27] A. Y. Purnama, B. E. Nurcahya, K. Nurhanafi, and R. Perdhana. (2021). "Mikrozonasi Berdasarkan Data Mikrotremor Dan Kecepatan Gelombang Geser Di Kotamadya Yogyakarta". *Positron.* **11** (2). 10.26418/positron.v11i2.46860.

[28] M. I. Nurwidyanto, M. Zainuri, A. Wirasatriya, and G. Yulianto. (2023). "Microzonation For Earthquake Hazards With HVSR Microtremor Method In The Coastal Areas Of Semarang Indonesia". *Geographia Technica.* **18** (1). 10.21163/GT_2023.181.13.

[29] S. P. Putti and N. Satyam. (2020). "Evaluation Of Site Effects Using HVSR Microtremor Measurements In Vishakhapatnam India". *Earth Systems and Environment.* **4** (2). 10.1007/s41748-020-00158-6.

[30] M. W. Asten, A. Askan, E. E. Ekincioglu, F. N. Sisman, and B. Ugurhan. (2014). "Site Characterisation In North Western Turkey Based On SPAC And HVSR Analysis Of Microtremor Noise". *Exploration Geophysics.* **45** (2). 10.1071/EG12026.

[31] V. L. Ipmawan, R. Prastowo, M. Iqbal, I. N. P. Permanasari, and S. Herman. (2025). "Effect Of Azimuthal Variability In Estimation Of HVSR Parameters And Ground Shear Strain At Kota Baru South Lampung Indonesia". *Journal of Science and Applicative Technology.* **9** (1). 10.35472/jsat.v9i1.2107.

[32] B. I. Siburian, M. Marzuki, and A. M. Lubis. (2024). "Local Site Effects And Seismic Microzonation Around Suban Area Curup Rejang Lebong Bengkulu Deduced By Ambient Noise Measurements". *Geoenvironmental Disasters.* **11** (1). 10.1186/s40677-024-00268-7.

[33] T. Rahayu, Z. Nasution, Roesyanto, and D. Karnawati. (2022). "Regional Zonation Based On Seismic Vulnerability Using Local Site Effect Analysis And Potential Damage To The City Of Medan North Sumatra Indonesia Due To Earthquake". *Geoenvironmental Disasters.* **9** (1). 10.1186/s40677-022-00227-0.

[34] P. Bard, A. Duval, A. Koehler, and S. Rao. (2004). "Guidelines For The Implementation Of The H V Spectral Ratio Technique On Ambient Vibrations Measurements Processing And Interpretation". SESAME European Research Project Site Effects Assessment Using Ambient Excitations.

[35] B. Roe. (2017). "Matter Density Versus Distance For The Neutrino Beam From Fermilab To Lead South Dakota And Comparison Of Oscillations With Variable And Constant Density". *Physical Review D.* **95** (11). 10.1103/PhysRevD.95.113004.

[36] K. Kanai. (1983). "Engineering Seismology". University of Tokyo Press, Tokyo.

[37] T. C. Amin, Sidarto, S. Santosa, and Gunawan. (1993). "Peta Geologi Lembar Kotaagung Sumatera Skala 1:250000". Pusat Penelitian dan Pengembangan Geologi, Bandung.

[38] S. Parolai, M. Picozzi, S. M. Richwalski, and C. Milkereit. (2005). "Joint Inversion Of Phase Velocity Dispersion And H V Ratio Curves From Seismic Noise Recordings Using A Genetic Algorithm Considering Higher Modes". *Geophysical Research Letters.* **32** (1). 10.1029/2004GL021115.